Journal of Biomechanical Engineering. Received March 08, 2018;
Accepted manuscript posted April 29, 2020. doi:10.1115/1.4047076

Research Article in *Journal of Biomechanical Engineering*

The Role of Fluid Shear and Metastatic Potential in Breast Cancer Cell Migration

Brandon D. Riehl[1], Eunju Kim[1], Jeong Soon Lee[1], Bin Duan[1,2,3], Ruiguo Yang,[1,2] Henry J. Donahue[4], Jung Yul Lim[1,2,*]

[1] Department of Mechanical and Materials Engineering, University of Nebraska-Lincoln, Lincoln, NE 68588, USA

[2] Mary and Dick Holland Regenerative Medicine Program, University of Nebraska Medical Center, Omaha, NE 68198, USA

[3] Division of Cardiology, Department of Internal Medicine, University of Nebraska Medical Center, Omaha, NE 68198, USA

[4] Department of Biomedical Engineering, Virginia Commonwealth University, Richmond, VA 23284, USA

* Corresponding: W317.3 Nebraska Hall, Department of Mechanical and Materials Engineering, University of Nebraska-Lincoln, Lincoln, NE 68588, USA; Fax: +1-402-472-1465; E-mail: jlim4@unl.edu (J.Y. Lim)

Journal of Biomechanical Engineering. Received March 08, 2018;
Accepted manuscript posted April 29, 2020. doi:10.1115/1.4047076

ABSTRACT

During the migration of cancer cells for metastasis, cancer cells can be exposed to fluid shear conditions. We examined two breast cancer cell lines, MDA-MB-468 (less metastatic) and MDA-MB-231 (more metastatic), and a benign MCF-10A epithelial cell line for their responsiveness in migration to fluid shear. We tested fluid shear at 15 dyne/cm^2 that can be encountered during breast cancer cells travelling through blood vessels or metastasizing to mechanically active tissues such as bone. MCF-10A exhibited the least migration with a trend of migrating in the flow direction. Intriguingly, fluid shear played a potent role as a trigger for MDA-MB-231 cell migration, inducing directional migration along the flow with significantly increased displacement length and migration speed and decreased arrest coefficient relative to unflowed MDA-MB-231. In contrast, MDA-MB-468 cells were markedly less migratory than MDA-MB-231 cells, and responded very poorly to fluid shear. As a result, MDA-MB-468 cells did not exhibit noticeable difference in migration between static and flow conditions, as was distinct in root mean square (RMS) displacement - an ensemble average of all participating cells. These may suggest that the difference between more metastatic MDA-MB-231 and less metastatic MDA-MB-468 breast cancer cells could be at least partly involved with their differential responsiveness to fluid shear stimulatory cues. Our study provides new data in regard to potential crosstalk between fluid shear and metastatic potential in mediating breast cancer cell migration.

Keywords: breast cancer, cell migration, fluid shear, metastatic potential

Journal of Biomechanical Engineering. Received March 08, 2018;
Accepted manuscript posted April 29, 2020. doi:10.1115/1.4047076

Introduction

Cancer metastasis and resulting complications are the primary cause of cancer related deaths. For women, breast cancer is the most common cancer which can metastasize to several organs including lung, liver, and bone. Despite the danger of breast cancer metastasis, the mechanisms underlying migration and invasion of breast cancer cells are not yet fully understood. In particular, while studies have revealed the effects of soluble factors on breast cancer cell migration (chemotaxis) [1-3], much remains to be learned about the regulatory role of mechanical environments. In general, mechanical loading milieus are important during the developmental process as they can regulate the initial morphogenesis; also in adulthood, mechanical loading can contribute to maintain cell/tissue homeostasis. Further, altered/interfered intra- and intercellular mechanical homeostasis can create maladaptation of tissues potentially driving disease progressions [4]. In this study, we examined how extracellular mechanical loading milieus, specifically fluid shear, will affect breast cancer cell migration.

Breast cancer metastasis is a multi-step process wherein cancer cells encounter unique fluid shear situations at varying stages of migration and metastasis. Breast cancer cells can be exposed to an increased pressure environment surrounding the breast tumor that produces interstitial outflow. Subsequent long-distance metastasis relies on breast cancer cells traveling through flow channels including vasculature. In blood vessels, breast cancer cells under flow may be free-floating or participate in rolling migration on the endothelial layer [1]. At the metastasis site, breast cancer cells can also interface with interstitial flow within the tissue. While shear force due to these fluid flows may be a dominant mechanical cue, how varying fluid shear situations regulate breast cancer cell migration is largely unknown. Improved understanding and

treatment of breast cancer metastasis may be revealed if the role of fluid shear in breast cancer cell migration could be elucidated.

Studies have evaluated the magnitudes of flow rates and shear stresses in cancer cell migration and metastasis environments. At the tumor site, increased pressure causes an increase in interstitial flow which drains to the lymph system, affecting cancer cell response and extracellular matrix (ECM) remodeling. Pathological interstitial flows typically have flow velocities greater than 1 μm/s, e.g., 55 μm/s reported for tumors in humans [5,6]. Shear stresses in the range of ca. 0.1 dyne/cm^2 are expected due to interstitial flow in the ECM and in the lumen of the lymph system with a peak stress of 12 dyne/cm^2 from lymph pump function [7]. In blood vessels, flow rates vary widely with small vessels having particularly high shear forces. Shear stresses up to 6 dyne/cm^2 are found in veins, and shear stresses up to 70 dyne/cm^2 are common in arteries [8]. Additionally, in breast cancer homing to other tissues such as bone, shear stresses of ca. 0.06 up to 30 dyne/cm^2 can be found due to the mechanically active bone microenvironment [9]. While considering these ranges, we chose 15 dyne/cm^2 shear stress in our test that may be encountered during breast cancer cell travelling through blood vessels or metastasis to tissues such as bone.

To examine the fluid shear control of breast cancer cell migration, we tested two established breast cancer cell lines, MDA-MB-231 and MDA-MB-468, and a benign epithelial cell line, MCF-10A, as a control. MCF-10A is established from primary breast tissue which expresses markers consistent with basal epithelial cells and lacks expressions of estrogen receptor (ER), progesterone receptor (PR), and human epidermal growth factor receptor 2 (HER2) [10]. This cell line is capable of forming acinar structures in culture, and unlike the cancer cell lines, is dependent on growth factors for survival [11]. Both MDA-MB-231 and

MDA-MB-468 breast cancer cell lines were established from pleural effusions and are negative for the therapeutic targets, ER, PR, and HER2 [12]. These cancer cell lines have been widely used as models of triple-negative breast cancer but with different classifications. The MDA-MB-468 cell line is classified as basal, not responsive to endocrine therapy, but may be responsive to chemotherapy; the MDA-MB-231 was initially classified as basal but is now classified as claudin-low [13]. The MDA-MB-231 line, in addition to having characteristics associated with epithelial-mesenchymal transition, has been likened to mammary cancer stem cells due to low expression of the proliferation marker Ki67 and $CD44^{+}$ $CD24^{-/low}$ [13]. Consequently, MDA-MB-231 breast cancer cells are known to be more aggressive and metastatic than MDA-MB-468 cells. We compared the migration of MCF-10A benign epithelial cells and MDA-MB-468 and MDA-MB-231 breast cancer cells under static and flow conditions to reveal the role of extracellular fluid shear cue and intrinsic metastatic potential in governing breast cancer cell migration. Our studies may provide a new insight into whether the difference in metastatic potential of breast cancer cells is at least partially related to a difference in cellular sensitivity to mechanical loads such as fluid shear.

Materials and Methods

Breast cancer cell lines. MDA-MB-231 (ATCC, CRM-HTB-26) and MDA-MB-468 (ATCC, HTB-132) cells were cultured using Dulbecco's Modified Eagle Medium (DMEM) supplemented with 10% fetal bovine serum (FBS) and 1% penicillin-streptomycin. For fluid shear tests, cells were seeded on a 25×75 mm^2 glass slide using 3×10^4 cells. The glass slide was not precoated with ECM proteins. The relatively small cell seeding number was to observe individual cell movement. After allowing cells to adhere on the glass slide for 8 h, medium was

replaced with serum reduced medium (5% FBS), and kept overnight before starting the flow test the next day. Our protocol of using media containing half the original serum concentration allows for maintaining sufficient protein for cell attachment and migration [14,15]. Although the use of serum starved media (0.5% FBS) can be adopted in large flow systems, we previously found that this concentration may be too low to support normal cell response to flow [16].

Benign epithelial cell line. MCF-10A (ATCC, CRL-10317) cells were cultured following the methods of Debnath et al. [10], using DMEM/F12 supplemented with 5% horse serum, 20 ng/ml epidermal growth factor (EGF), 0.5 µg/ml hydrocortisone, 100 ng/ml cholera toxin, 10 µg/ml insulin, and 1% penicillin-streptomycin. MCF-10A cells were cultured and flowed on the glass slides following the same protocol described above for breast cancer cell lines. Serum reduced flow media consisted of DMEM/F12 supplemented with 2.5% horse serum and 1% penicillin-streptomycin.

Applying fluid flow to cells. Using a parallel plate flow chamber, we applied steady laminar flow to cells seeded on the glass slide. Fluid shear experienced by the cells is the wall shear stress of the parallel plate chamber. The shear stress could be adjusted by the flow rate (ml/min) imposed by the device. Cell lines were exposed to flow at 15 dyne/cm^2 shear stress (labeled as FF15), or placed in the same chamber but not exposed to flow (static control). We used 15 dyne/cm^2 as one physiologically relevant shear stress as described above. The flow tests were conducted using a flow device (Flexcell) following our published protocols [14-18]. Briefly, the flow loop was made with Masterflex L/S 16 tubing that connects the media reservoir, peristaltic pump, Osci-flow controller, two pulse dampeners, and the FlexFlow chamber through which cell migration can be observed (Fig. S1). Steady flow at a given flow rate was achieved by the StreamSoft software. The flow channel was sterilized with 70% ethanol and flushed with

deionized water. Then, serum reduced (5% FBS or 2.5% horse serum for breast cancer and benign cells, respectively) flow medium was added to the reservoir which was maintained at 37°C in a water bath. Next, bubbles in the tubing were purged and a leak test was performed before attaching cell-seeded glass slide to the flow chamber with a vacuum pump. Flow medium was primed through the loop to remove bubbles that may have occurred during the chamber assembly. A minimum of 3 slides per each test condition were prepared and a minimum of 20 trackable cells were quantified for each experimental condition.

Time lapse imaging of cell migration. We placed the flow chamber on an inverted Leica DMI 4000 microscope, and phase contrast images were recorded every min for 2 h for both static and flow conditions. To correct for device drift, the template matching plugin in Fiji-ImageJ software [19] was used. Stabilized images were segmented in Time Lapse Analyzer (TLA) to obtain binary masks for each image using Sobel edge detection [20] (see Table S1 for image processing stack). The binary masks were tracked in TLA and our custom MATLAB scripts were used to quantify cell migration. All these methods followed the protocols we recently developed [14,15].

Quantification of cell migration parameters. We quantified cell migration parameters including displacement, migration speed, arrest coefficient, root means square (RMS) displacement, etc. In TLA, cell centroids were determined from the cell outlines at each time frame of measurement. Connection of the centroid positions produced raw cell migration tracks which were processed using custom-written MATLAB. Then, the linear distance from the starting centroid position to the final one was defined as the displacement. Cell speed was also calculated at each time frame. We further assessed whether cells migrated with or against the given flow direction, and measured path and time efficiency during migration. The confinement

ratio, defined as the displacement divided by the total path length, was used to assess how straight the migration path is. The arrest coefficient measured the percent of time a cell paused during the migration: a cell was considered paused if the cell speed was less than one standard deviation below the average speed of the (less migratory) MDA-MB-468 breast cancer cells under static condition (i.e., 0.1735 μm/min). Finally, RMS displacement was used to evaluate the overall cell migration behavior as a holistic measure. The RMS displacement is an ensemble average of displacements for the entire participating cells defined as $X(t)_{RMS}$:

$$X(t)_{RMS} = \sqrt{\frac{1}{N}\sum_{i=1}^{N}[x_i(t) - x_i(0)]^2}$$

where N is the total number of cells and $x_i(t)$ is the position of the i-th cell at time t. From the slope of the RMS displacement vs. time$^{1/2}$ plot, the motility coefficient could be calculated as a strength measure of cell migration, which is analogous to the diffusion coefficient of the first order diffusion kinetics [14,15].

Statistics. Our results were processed in MATLAB with one way analysis of variance (ANOVA) with a Tukey-Kramer post-hoc test for statistical significance. All statistical assumptions of ANOVA were verified and the data were log10 transformed, tested, and back transformed if necessary to adjust for data that violated the normally-distributed assumption (Table S2). All results are presented as mean ± standard error of measurement (SEM).

Results

MDA-MB-231 cells detach more under fluid shear. The first step we took before assessing cell migration parameters was to quantify the percentage of cells that remain attached on the substrate under fluid flows. Cells that remained in the viewing frame during the time lapse

Journal of Biomechanical Engineering. Received March 08, 2018;
Accepted manuscript posted April 29, 2020. doi:10.1115/1.4047076

imaging were considered to be undergoing crawling migration and used for analyses. MCF-10A cells had secure attachment to the slides with 3% detaching in the static group and 9% detaching by 15 dyne/cm^2 shear. Among breast cancer cell lines, MDA-MB-468 had the greater tendency to remain attached to the slide than MDA-MB-231 cells. MDA-MB-468 showed 3% and 10% detachments in the static and flow groups, respectively. On the other hand, MDA-MB-231 cells had 6% detaching under static condition and surprisingly 52% detachment by 15 dyne/cm^2 fluid shear. It may be inferred from this difference that the MDA-MB-231 cell line is less likely to remain attached when exposed to flow-induced shear and may readily participate in long-distance migration by free-floating. Note, cells that detached from the substrate may or may not participate in active migration, analysis of which was beyond the scope of the current study.

MDA-MB-231 cells show strong fluid shear-dependent migration relative to MDA-MB-468 and MCF-10A. Observed original tracks of crawling cell migration are shown in Fig.1a for the benign cells (MCF-10A) and in Fig. 2a for two breast cancer cell lines (MDA-MB-468 and MDA-MB-231). In these figures, each cell tracks were shifted to the center of the plot for comparison. The directional tendency of cell migration can be better visualized in the displacement vector plots (Figs. 1b, 2b) and migration angle histograms (Figs. 1c, 2c). Benign epithelial MCF-10A cells displayed random migration under static condition but a noticeable bias to the flow direction under fluid shear (Fig. 1c). This may establish a baseline of cell migration and its shear sensitivity to which the cancer cell lines can be compared.

Under static condition, both MDA-MB-468 and MDA-MB-231 cells were relatively less mobile and showed migration in random directions (Fig. 2a). Interestingly, fluid shear resulted in directed migration of MDA-MB-231 cells along the flow direction, while this effect appeared to be less pronounced for MDA-MB-468 cells (Fig. 2b,c). When quantified based on the criteria of

with or against the flow (within $\pi/8$ angle of the flow or to the opposite direction, Fig. 2d), MDA-MB-231 cells displayed notably increased directionality, e.g., significantly larger percentage of MDA-MB-231 cells moving with flow (Fig. 2e). Percentage cells moving against the flow was not different among test conditions. In another measure, there was no significant difference in the time spent moving with the flow, but unexpectedly, MCF-10A and MDA-MB-231 cells spent more time moving against the flow (Fig. 2f). This might be related to increased cell motility under shear. Especially for MDA-MB-231 cells, while they moved with the flow as a whole, the tendency to continuously move under flow stimulation also resulted in increased time spent moving against the flow. Similar directional migration trends were observed in the breast cancer cell lines when assessed up to 1 h (Fig. S2). Combined data indicate that (more metastatic) MDA-MB-231 cells were highly responsive to fluid shear at 15 dyne/cm^2 whereas (less metastatic) MDA-MB-468 cells were less or not responsive to the fluid shear.

MDA-MB-231 cells have greater displacement length under flow due to less arrest. Quantification of cell migration showed that sheared MDA-MB-231 cells had increased displacement and uninterrupted migration. The MDA-MB-231 line under flow migrated significantly farther than MDA-MB-468 and MCF-10A cells (Fig. 3a). This difference in cell displacement could be influenced by increased path efficiency (Fig. 3b, confinement ratio measuring how straight the path is) but more strongly affected by the persistence in migration (Fig. 3c, arrest coefficient measuring how often cells stop). Overall, the migration of MDA-MB-231 was more aggressive in both static and sheared groups in that it stopped less than the other cells, which trait was even increased under flow with sheared MDA-MB-231 spending the least time paused. The benign MCF-10A cell line had the least displacement and confinement ratio of the three cell lines tested in both static and sheared conditions.

Cell migration speed changes with cell type, flow, and time of measurement. In the first minute after shear onset, the migration speed of the flowed MCF-10A cell line was significantly higher than its static counterpart, but it quickly dropped to the similar levels as the static group (Fig. 4a). MDA-MB-231 cells showed similar but even more pronounced changes in migration speed mostly during the initial periods of measurement (Fig. 4b without error bars for easy viewing; see Fig. S3 with error bars; Fig. 4c up to 30 min for comparison). In Fig. 4c, the aggressive nature of MDA-MB-231 cells was evident in the migration speed. The average speed of MDA-MB-231 cells in both static and fluid sheared conditions tended to be greater than those of MDA-MB-468 cells, of which the change was greater in response to shear. For MDA-MB-468 cells, no significant increase in migration speed was observed even when stimulated with shear. In fact, sheared MDA-MB-468 showed at times less speed than its own counterpart, static MDA-MB-468. The migration speed showed, in overall, consistent results with the observations of percentage of cells migrating with flow, displacement, and arrest coefficient.

Difference in migration tendency for MCF-10A, MDA-MB-468, and MDA-MB-231 cells is evident in RMS ensemble average. RMS displacement, a holistic measure of cell migration tendency as an ensemble average for all participating cells [14,15], is quantified and compared for the six test groups (Fig. 5). As revealed by RMS plots, static and sheared MCF-10A cells had the least group migration among three cell lines tested. The MCF-10A static group had the lowest overall RMS displacement values, followed by the MCF-10A sheared group when assessed at the end of the measurement time. It is noticeable that flowed MCF-10A cells showed initial fluid shear response and then decrease, which results in less RMS displacement than MDA-MB-468 groups at the end of the measurement. Interestingly, both the static and sheared MDA-MB-468 cases displayed remarkably similar trends in RMS displacements, which can be a

clear evidence that MDA-MB-468 cells respond poorly to fluid shear stimulation. As a result, RMS displacements of both static and flowed MDA-MB-468 groups were even less than the MDA-MB-231 static case. Among all test conditions, sheared MDA-MB-231 cells had the greatest propensity for migration with RMS displacements much greater than all the other cases. The motility coefficients (slope of the RMS plot analogous to the diffusion coefficient of the first order diffusion kinetics [14,15]) were calculated to quantify the overall strength of migration. MCF-10A displayed low motility coefficients, 0.14 and 0.12 for static and sheared conditions, respectively. MDA-MB-468 cells exhibited the motility coefficient of 0.54, the same values for both static and sheared cases, again indicating that MDA-MB-468 cell migration may not be affected by flow. The MDA-MB-231 line under static condition produced a motility coefficient of 0.52 but greater terminal RMS displacement than both the MDA-MB-468 cases, potentially due to initial strong migration of MDA-MB-231 at the experimental onset (also see Fig. 4c). Sheared MDA-MB-231 cells exhibited the greatest motility coefficient of 1.50 (almost tripled relative to the other conditions), indicating the highest flow sensitivity in migration among test cases. The mean squared displacement (MSD), another presentation of cell migration in a collective sense accounting for both ensemble and time averaging [14] (see equation and MSD plot in Fig. S4), showed trends similar to the RMS plot.

Discussion

In addition to soluble factor-driven cell migration (chemotaxis), revealing the spread of metastasizing cancer cells due to mechanical factors such as fluid shear may be of significance in understanding what triggers and facilitates cancer metastasis. For low shear stress, as may be encountered in the lymph system, the chemotactic response and shear stress regulation can be

interlinked. For example, at low flow rates, autologous chemotaxis regulated by shear response has been observed in breast cancer lymphatic metastasis [21]. Our results demonstrate that the fluid shear environment at relatively high stress may also play a regulatory role in breast cancer cell migration. In vivo, pressure is built up around tumors accompanying interstitial outflows. Flows are also encountered in vascular and lymph systems and in other microchannels within the target tissues to which cancer cells metastasize. For instance, breast cancer cells can be exposed to flow shear within the bone, one of the primary metastasis sites of breast cancer cells. Here we observed that fluid flow can increase breast cancer cell migration, but triggering by shear may be mediated by the intrinsic metastatic potential of the breast cancer cells. Note, our observed differences in breast cancer cell migration may be unlikely due to differences in cell spreading area (and resultant fluid drag), as no significant differences in cell area were found between two breast cancer cell lines (Fig. S5). The MDA-MB-468 line with lower metastatic potential had significantly less migration in both static and sheared conditions compared with more metastatic MDA-MB-231 line. The benign MCF-10A cell line had the least migration among the three cell lines tested in both static and sheared conditions. MCF-10A cells demonstrated a slight response to shear with a small increase in cell migration along the flow. Interestingly, MDA-MB-468 cells were found to be unresponsive to shear stimulation, suggesting that the less metastatic nature of MDA-MB-468 cells may be correlated with their insensitivity to mechanical signals. In contrast to MDA-MB-468, MDA-MB-231 cells exhibited potent migration capacity even under static condition. Further, MDA-MB-231 cells responded strongly to shear, resulting in significantly increased migration parameters (percentage cells migrating with flow, displacement, cell speed, etc.) with less stops. The combined trend of stimulated migration under flow for MDA-MB-231 could be more clearly demonstrated in the RMS displacement plot.

The fluid shear-induced directional migration of breast cancer cells is not clearly understood yet. In our study, MDA-MB-231 cells preferentially migrated along with the flow direction. This may be in contrast to the study by Huang et al. [6], in which no preferential migration direction was observed for MDA-MB-231 cells embedded in a collagen matrix and exposed to interstitial flows. In the study by Polacheck et al. [22], the preference of breast cancer cell migration may depend on the cell seeding density: interstitial flow within a collagen matrix caused breast cancer cells to migrate with the flow direction when seeded at a low density, but caused migration against the flow at a high density. Our test differs from these studies in that we used stiff glass slides as basal substrate with no ECM coating with applying well-controlled wall shear stress between parallel plates. It is likely that the directional preference of cell migration under flow can be in general influenced by multiple factors including the composition of the migration test substrate (glass or collagen), cell density, 2D vs. 3D flows, etc. [23]. Under 3D environment mimicking interstitial flows [24], a heterogeneous response of MDA-MB-231 was observed: shear increased the cell migration speed but caused subpopulations of the cells to migrate with or against the flow direction. Taken together, this suggests a need for a more systematic study that explores a variety of extracellular culture environments to better resemble in vivo fluid shear milieus and to mimic the biochemical and mechanobiological characteristics of the metastasis tissue.

Studies on cancer mechanobiology have proposed that maladaptation in cell mechanical homeostasis may contribute to increased metastasis. For example, highly metastatic breast cancers may have higher synthesis of glycocalyx cell coating proteins, which is implicated in interstitial flow mechanotransduction, regulation of ECM degrading factor, and cell surface shear magnification [25,26]. It was reported shear stress increased tumor cell motility and upregulated

matrix degrading factors [26]. Also, when glycocalyx-degrading factors were applied, the shear-induced responses were abolished, revealing a potential therapeutic target. Via these glycocalyx-mediated responses the cancer becomes more invasive while also increasing sensitivity to the mechanical loading environment. Additionally, the presence of tumors alters the solid stress environment to create non-physiological stress building up to 10 times in the interstitial pressure. Relevant loading cues, such as compressive strain, have been shown to alter metastasis-relevant genes in the MDA-MB-231 cells within 3D tumor analogs in vitro [27]. Another study showed that compromised mechano-reciprocity may cause a disruption in mechanical homeostasis by interfering with cells' sensing of mechanical environment and altering cellular stiffness [28]. In that study, ex vivo cultured cancer cells actually displayed significantly lower cell stiffness. This change in cancer cell stiffness can be terminally correlated with the metastatic potential [29]. Our study provides additional evidence that mechanical environments may crosstalk with cancer cell physiology.

Breast cancer cells have been shown to have differential integrin-ECM interactions [30-32]. Cell adhesion to ECM is mediated through combinations of α and β integrin subunits with specific combinations having affinity for specific ECM proteins. Since we did not precoat the glass substrates with ECM proteins such as collagen, cell attachment to uncoated glass slides could occur through binding to adsorbed serum proteins such as vitronectin or fibronectin, as was the report for MDA-MB-231 cells [30]. Cell attachment to vitronectin and fibronectin can both be mediated by integrin αvβ3 which has high expression in cancerous epithelial cells compared with healthy cells. Adhesion to fibronectin is also mediated by αvβ6 integrin in malignant epithelial cells. Differential expression of integrins may have an effect on breast cancer cell adhesion and the crawling migration. For the cells tested in this study, interestingly,

MDA-MB-231 attachment to fibronectin was primarily dependent on αvβ3 whereas MDA-MB-468 and MCF-10A were dependent on αvβ6 [31]. Overall, metastatic cells have been identified to have lower adhesion than non-metastatic or benign cell lines [30]. This can be also correlated with our data on more MDA-MB-231 cell detachment under fluid shear. Combined, this may suggest one hallmark of cancer, where anchorage and integrin-dependent anoikis is bypassed. For example, MDA-MB-468 cells have been shown to have multiple phenotypes with adherent and non-adherent subpopulations [32].

Cell migration is a highly coordinated effort of focal adhesion-cytoskeletal remodeling with regulated contraction and protrusion of the cell membrane. When subjected to shear, mechanotransduction related to focal adhesion can be activated. Shearing MDA-MB-231 cells established a gradient of β1 integrin, vinculin, and focal adhesion kinase (FAK) activation, and these changes were associated with altered cell tension, polarization, and migration [33]. Mechanosensors related to cytoskeletal remodeling can also affect cancer cell migration. For instance, blocking NEDD9 and RhoA kinase (ROCK) could impair possible modes of triple-negative breast cancer (TNBC) cell migration, e.g., amoeboid or mesenchymal migration mode [34]. This result on ROCK control of cancer cell migration may be in contrast to those on mesenchymal stem cells [14] and osteoblasts [15] that showed increased cell migration under ROCK silencing. Since ROCK expression in breast cancer cells may also be affected by other cues such as hypoxia [35], a test may need to combine such aspects of tumor maladaptation, e.g., flow tests under hypoxia.

More studies on varying shear stress levels are also needed, which will give a more comprehensive understanding of cancer cell migration as many different fluid flow speeds (thus varying shear stresses) exist within the body depending on the location of blood vessel, lymph

system, and the metastasizing target tissue type. Another new avenue open for exploration would be measuring grouped cell migration behavior. While individual cell migration under flow was assessed in this study, cancer cells in vivo will often be clumped together and collectively migrate while maintaining cell-cell junctions [36].

In conclusion, in our study comparing the migration of two human breast cancer cell lines, MDA-MB-468 (less metastatic) and MDA-MB-231 (more metastatic), and a benign epithelial cell line, MCF-10A, under fluid flow-induced shear, it was observed that both fluid shear stress environment and intrinsic metastatic potential of breast cancer cells affect their migration behavior. Shear stress was a potent migration trigger for MDA-MB-231 cells causing increased directional migration along the flow direction with increased displacement and speed and decreased arrest. In contrast, MCF-10A had low migratory potential, and MDA-MB-468 cells were unresponsive to shear and had significantly less migration than MDA-MB-231 cells. The data may suggest that difference in metastatic potential may be at least partially correlated with difference in cellular sensitivity to mechanical loading milieus such as fluid shear. Further revealing the mechanotransduction cascades involved in different migration would contribute to future cancer treatments.

Acknowledgements

We thank the funding support given to Bin Duan from AHA Scientist Development Grant (17SDG33680170, PI: Duan); funding given to Ruiguo Yang from NIH/NIGMS Nebraska Center for Integrated Biomolecular Communication (NCIBC) (P20GM113126, PI: Takacs), NIH/NIGMS Nebraska Center for Nanomedicine (P30GM127200, PI: Bronich), NSF grant (1826135, PI: Yang), and Nebraska Collaborative Initiative (PI: Yang); funding given to Jung

Yul Lim from NIH/NIGMS Nebraska Center for the Prevention of Obesity Diseases (NPOD) Seed Grant (P20GM104320, PI: Zempleni) and NIH/NIGMS Great Plains IDeA-CTR Pilot Grant (1U54GM115458-01, PI: Rizzo).

Supplementary data

Supplementary data are provided.

References

[1] Leber, M. F., Efferth, T., 2009, "Molecular Principles of Cancer Invasion and Metastasis (Review)," Int. J. Oncol., **34**(4), pp. 881-895.

[2] Mareel, M., Leroy, A., 2003, "Clinical, Cellular, and Molecular Aspects of Cancer Invasion," Physiol. Rev., **83**(2), pp. 337-376.

[3] Arrigoni, C., Bersini, S., Gilardi, M., Moretti, M., 2016, "In Vitro Co-culture Models of Breast Cancer Metastatic Progression towards Bone," Int. J. Mol. Sci., **17**(9), pp. E1405.

[4] Butcher, D. T., Alliston, T., Weaver, V. M., 2009, "A Tense Situation: Forcing Tumour Progression," Nat. Rev. Cancer, **9**(2), pp. 108-122.

[5] Swartz, M. A., Lund, A. W., 2012, "Lymphatic and Interstitial Flow in the Tumour Microenvironment: Linking Mechanobiology with Immunity," Nat. Rev. Cancer, **12**(3), pp. 210-219.

[6] Huang, Y. L., Tung, C. K., Zheng, A., Kim, B. J., Wu, M., 2015, "Interstitial Flows Promote Amoeboid over Mesenchymal Motility of Breast Cancer Cells Revealed by a Three Dimensional Microfluidic Model," Integr. Biol. (Camb.), **7**(11), pp. 1402-1411.

[7] Wiig, H., Swartz, M. A., 2012, "Interstitial Fluid and Lymph Formation and Transport: Physiological Regulation and Roles in Inflammation and Cancer," Physiol. Rev., **92**(3), pp. 1005-1060.

[8] Malek, A. M., Alper, S. L., Izumo, S., 1999, "Hemodynamic Shear Stress and Its Role in Atherosclerosis," JAMA, **282**(21), pp. 2035-2042.

[9] Orr, D. E., Burg, K. J. L., 2008, "Design of a Modular Bioreactor to Incorporate Both Perfusion Flow and Hydrostatic Compression for Tissue Engineering Applications," Ann. Biomed. Eng., **36**(7), pp. 1228-1241.

[10] Debnath, J., Muthuswamy, S. K., Brugge, J. S., 2003, "Morphogenesis and Oncogenesis of MCF-10A Mammary Epithelial Acini Grown in Three-Dimensional Basement Membrane Cultures," Methods, **30**(3), pp. 256-268.

[11] Neve, R. M., Chin, K., Fridlyand, J., Yeh, J., Baehner, F. L., Fevr, T., Clark, L., Bayani, N., Coppe, J. P., Tong, F., Speed, T., Spellman, P. T., DeVries, S., Lapuk, A., Wang, N. J., Kuo, W. L., Stilwell, J. L., Pinkel, D., Albertson, D. G., Waldman, F. M., McCormick, F., Dickson, R. B., Johnson, M. D., Lippman, M., Ethier, S., Gazdar, A., Gray, J. W., 2006, "A

Collection of Breast Cancer Cell Lines for the Study of Functionally Distinct Cancer Subtypes," Cancer Cell, **10**(6), pp. 515-527.

[12] Cailleau, R., Olivé, M., Cruciger, Q. V., 1978, "Long-term Human Breast Carcinoma Cell Lines of Metastatic Origin: Preliminary Characterization," In Vitro, **14**(11), pp. 911-915.

[13] Holliday, D. L., Speirs, V., 2011, "Choosing the Right Cell Line for Breast Cancer Research," Breast Cancer Res., **13**(4), pp. 215.

[14] Riehl, B. D., Lee, J. S., Ha, L., Lim, J. Y., 2015, "Fluid-flow-induced Mesenchymal Stem Cell Migration: Role of Focal Adhesion Kinase and RhoA Kinase Sensors," J. R. Soc. Interface, **12**(104), pp. 20141351.

[15] Riehl, B. D., Lee, J. S., Ha, L., Kwon, I. K., Lim, J. Y., 2017, "Flowtaxis of Osteoblast Migration under Fluid Shear and the Effect of RhoA Kinase Silencing," PLoS One, **12**(2), pp. e0171857.

[16] Riddle, R. C., Hippe, K. R., Donahue, H. J., 2008, "Chemotransport Contributes to the Effect of Oscillatory Fluid Flow on Human Bone Marrow Stromal Cell Proliferation," J. Orthop. Res., **26**(7), pp. 918-924.

[17] Salvi, J. D., Lim, J. Y., Donahue, H. J., 2010, "Increased Mechanosensitivity of Cells Cultured on Nanotopographies," J. Biomech., **43**(15), pp. 3058-3062.

[18] Salvi, J. D., Lim, J. Y., Donahue, H. J., 2010, "Finite Element Analyses of Fluid Flow Conditions in Cell Culture," Tissue Eng. Part C Methods. **16**(4), pp. 661-670.

[19] Schindelin, J., Arganda-Carreras, I., Frise, E., Kaynig, V., Longair, M., Pietzsch, T., Preibisch, S., Rueden, C., Saalfeld, S., Schmid, B., Tinevez, J. Y., White, D. J., Hartenstein, V., Eliceiri, K., Tomancak, P., Cardona, A., 2012, "Fiji: an Open-Source Platform for Biological-image Analysis," Nat. Methods, **9**(7), pp. 676-682.

[20] Huth, J., Buchholz, M., Kraus, J. M., Schmucker, M., von Wichert, G., Krndija, D., Seufferlein, T., Gress, T. M., Kestler, H. A., 2010, "Significantly Improved Precision of Cell Migration Analysis in Time-lapse Video Microscopy through Use of a Fully Automated Tracking System," BMC Cell Biol., **11**, pp. 24.

[21] Shields, J. D., Fleury, M. E., Yong, C., Tomei, A. A., Randolph, G. J., Swartz, M. A., 2007, "Autologous Chemotaxis as a Mechanism of Tumor Cell Homing to Lymphatics via Interstitial Flow and Autocrine CCR7 Signaling," Cancer Cell, **11**(6), pp. 526-538.

[22] Polacheck, W. J., Charest, J. L., Kamm, R. D., 2011, "Interstitial Flow Influences Direction of Tumor Cell Migration through Competing Mechanisms," Proc. Natl. Acad. Sci. U.S.A., **108**(27), pp. 11115-11120.

[23] Andalib, M. N., Dzenis, Y., Donahue, H. J., Lim, J. Y., 2016, "Biomimetic Substrate Control of Ccellular Mechanotransduction," Biomater. Res., **20**, pp. 11.

[24] Haessler, U., Teo, J. C., Foretay, D., Renaud, P., Swartz, M. A., 2012, "Migration Dynamics of Breast Cancer Cells in a Tunable 3D Interstitial Flow Chamber," Integr. Biol., **4**(4), pp. 401-409.

[25] Tarbell, J. M., Cancel, L. M., 2016, "The Glycocalyx and Its Significance in Human Medicine," J. Intern. Med., **280**(1), pp. 97-113.

[26] Qazi, H., Palomino, R., Shi, Z. D., Munn, L. L., Tarbell, J. M., 2013, "Cancer Cell Glycocalyx Mediates Mechanostransduction and Flow-Regulated Invasion," Integr. Biol., **5**(11), pp. 1334-1343.

[27] Demou, Z. N., 2010, "Gene Expression Profiles in 3D Tumor Analogs Indicate Compressive Strain Differentially Enhances Metastatic Potential," Ann. Biomed. Eng., **38**(11), pp. 3509-3520.

[28] Cross, S. E., Jin, Y. S., Rao, J., Gimzewski, J. K., 2007, "Nanomechanical Analysis of Cells from Cancer Patients," Nat. Nanotechnol., **2**(12), pp. 780-783.

[29] Suresh, S., 2007, "Biomechanics and Biophysics of Cancer Cells," Acta Biomater., **3**(4), pp. 413-438.

[30] Taherian, A., Li, X., Liu, Y., Haas, T. A., 2011, "Differences in Integrin Expression and Signaling within Human Breast Cancer Cells," BMC Cancer, **11**, pp. 293.

[31] Singh, C., Shyanti, R. K., Singh, V., Kale, R. K., Mishra, J. P. N., Singh, R. P., 2018, "Integrin Expression and Glycosylation Patterns Regulate Cell-Matrix Adhesion and Alter with Breast Cancer Progression," Biochem. Biophys. Res. Commun., **499**(2), pp. 374-380.

[32] Veß, A., Blache, U., Leitner, L., Kurz, A. R. M., Ehrenpfordt, A., Sixt, M., and Posern, G., 2017, "A Dual Phenotype of MDA-MB-468 Cancer Cells Reveals Mutual Regulation of Tensin3 and Adhesion Plasticity," J. Cell Sci., **130**(13), pp. 2172-2184.

[33] Polacheck, W. J., German, A. E., Mammoto, A., Ingber, D. E., Kamm, R. D., 2014, "Mechanotransduction of Fluid Stresses Governs 3D Cell Migration," Proc. Natl. Acad. Sci. U.S.A., **111**(7), pp. 2447-2452.

[34] Jones, B. C., Kelley, L. C., Loskutov, Y. V., Marinak, K. M., Kozyreva, V. K., Smolkin, M. B., Pugacheva, E. N., 2017, "Dual Targeting of Mesenchymal and Amoeboid Motility Hinders Metastatic Behavior," Mol. Cancer Res., **15**(6), pp. 670-682.

[35] Gilkes, D. M., Xiang, L., Lee, S. J., Chaturvedi, P., Hubbi, M. E., Wirtz, D., Semenza, G. L., 2014, "Hypoxia-inducible Factors Mediate Coordinated RhoA-ROCK1 Expression and Signaling in Breast Cancer Cells," Proc. Natl. Acad. Sci. U.S.A., **111**(3), pp. E384-E393.

[36] Mayor, R., Etienne-Manneville, S., 2016, "The Front and Rear of Collective Cell Migration", Nat. Rev. Mol. Cell Biol., **17**(2), pp. 97-109.

Fig. 1. Tracking of benign MCF-10A epithelial cells reveals random cell migration with less strong shear stress response. (a) Individual cells were tracked and plotted with track initiation shifted to the plot origin. Each color represents a distinct cell migration path. A slight bias of cell migrating along the flow direction is seen in (b) the vector plot and (c) the angle histogram.

Fig. 2. Fluid shear triggers MDA-MB-231 cell migration in the flow direction but does not affect MDA-MB-468 cell. (a) Under static condition, no directional preference was found for either MDA-MB-231 or MDA-MB-468 cell lines. Directional migration for sheared MDA-MB-231 cells is seen in (b) which has migration tracks replaced by the resultant vector and (c) an angle histogram. (d) Diagram illustrating definition of migration with and against flow direction. (e) The percent of cells moving with and against the flow direction. (f) Time migrating with and against the flow direction. #: comparison with MCF-10A static. *: comparison with MDA-MB-468 static. Other comparisons did not reach statistical significance. Single and triple symbols represent $p < 0.05$ and $p < 0.001$ respectively.

Fig. 3. Migration displacement and persistence, potential measures of breast cancer cell invasiveness, increase under shear but only for MDA-MB-231 cells. (a) Sheared MDA-MB-231 cells migrated significantly farther than MDA-MB-468 and MCF-10A cells. Interestingly, this was not likely due to an increased path efficiency (b) because there was little difference in confinement ratio. (c) MDA-MB-231 cells had greater persistence in migration (or lower arrest) in both static and sheared conditions compared with MDA-MB-468 and MCF-10A cells. Application of shear further decreased the arrest coefficient of MDA-MB-231 cells causing more persistent migration. #: comparison with MCF-10A static. ψ: comparison with MCF-10A FF15. *: comparison with MDA-MB-468 static. ‡: comparison with MDA-MB-468 FF15. Other comparisons did not reach statistical significance. Single, double, and triple symbols represent $p < 0.05$, $p < 0.01$, and $p < 0.001$ respectively.

Fig. 4. Breast cancer cell migration speed is dependent on metastatic potential, shear stimulation, and time after shear. (a) MCF-10A exhibited low response to flow stimulation with only an increase in cell speed at shear onset. (b,c) The MDA-MB-231 line may exhibit characteristics related to increased metastasis by migrating significantly faster than MDA-MB-

468. The greatest speed of the MDA-MB-231 line was seen at shear onset with the speed decreasing until reaching a rather constant value after about 30 min. #: comparison with MCF-10A static. *: comparison with MDA-MB-468 static. ‡: comparison with MDA-MB-468 FF15. +: comparison with MDA-MB-231 static. Other comparisons did not reach statistical significance. Single, double, and triple symbols represent $p < 0.05$, $p < 0.01$, and $p < 0.001$ respectively.

Fig. 5. Intrinsic metastatic potential and extracellular fluid shear may combine to increase breast cancer cell migration. RMS displacement is a measure of cell migration in a collective sense that ensemble-averages and thus summarizes overall migration trends. The MCF-10A cells had the lowest RMS displacement in both static and sheared conditions, reflecting the low migration capabilities of the benign cells. The MDA-MB-468 line was unaffected by fluid shear stimulation with almost indistinguishable differences in the static and sheared cases. The MDA-MB-231 line under static condition had higher RMS displacement compared with MDA-MB-468 line under static and flow conditions. Shear stimulation significantly activated MDA-MB-231 cell migration resulting in highest RMS displacement.

Journal of Biomechanical Engineering. Received March 08, 2018;
Accepted manuscript posted April 29, 2020. doi:10.1115/1.4047076

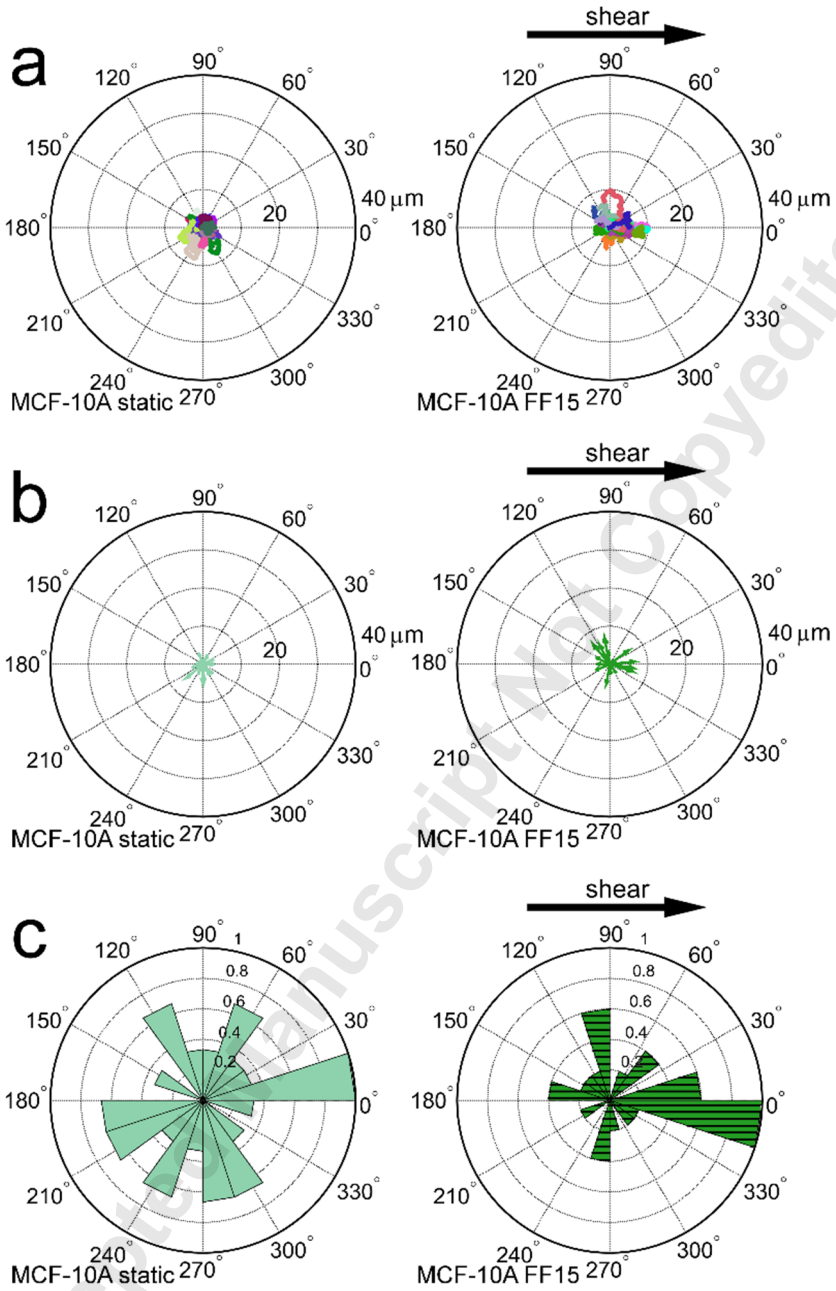

Fig. 1

Journal of Biomechanical Engineering. Received March 08, 2018;
Accepted manuscript posted April 29, 2020. doi:10.1115/1.4047076

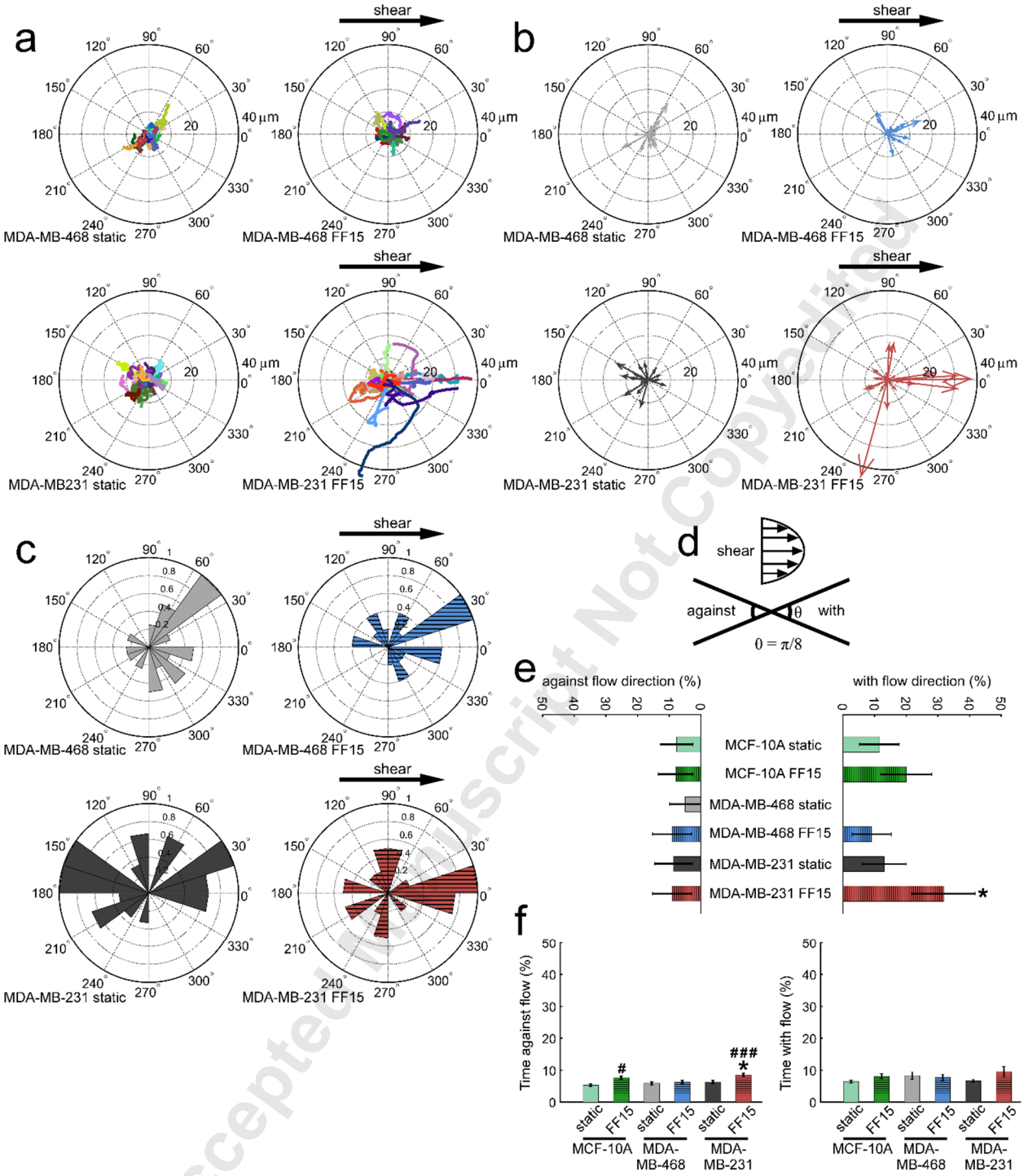

Fig. 2

Journal of Biomechanical Engineering. Received March 08, 2018;
Accepted manuscript posted April 29, 2020. doi:10.1115/1.4047076

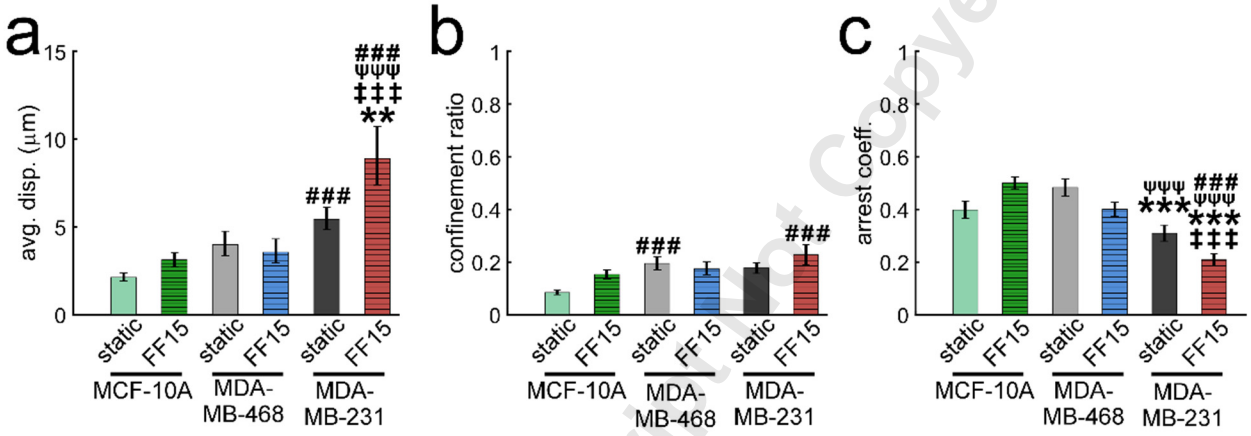

Fig. 3

Journal of Biomechanical Engineering. Received March 08, 2018;
Accepted manuscript posted April 29, 2020. doi:10.1115/1.4047076

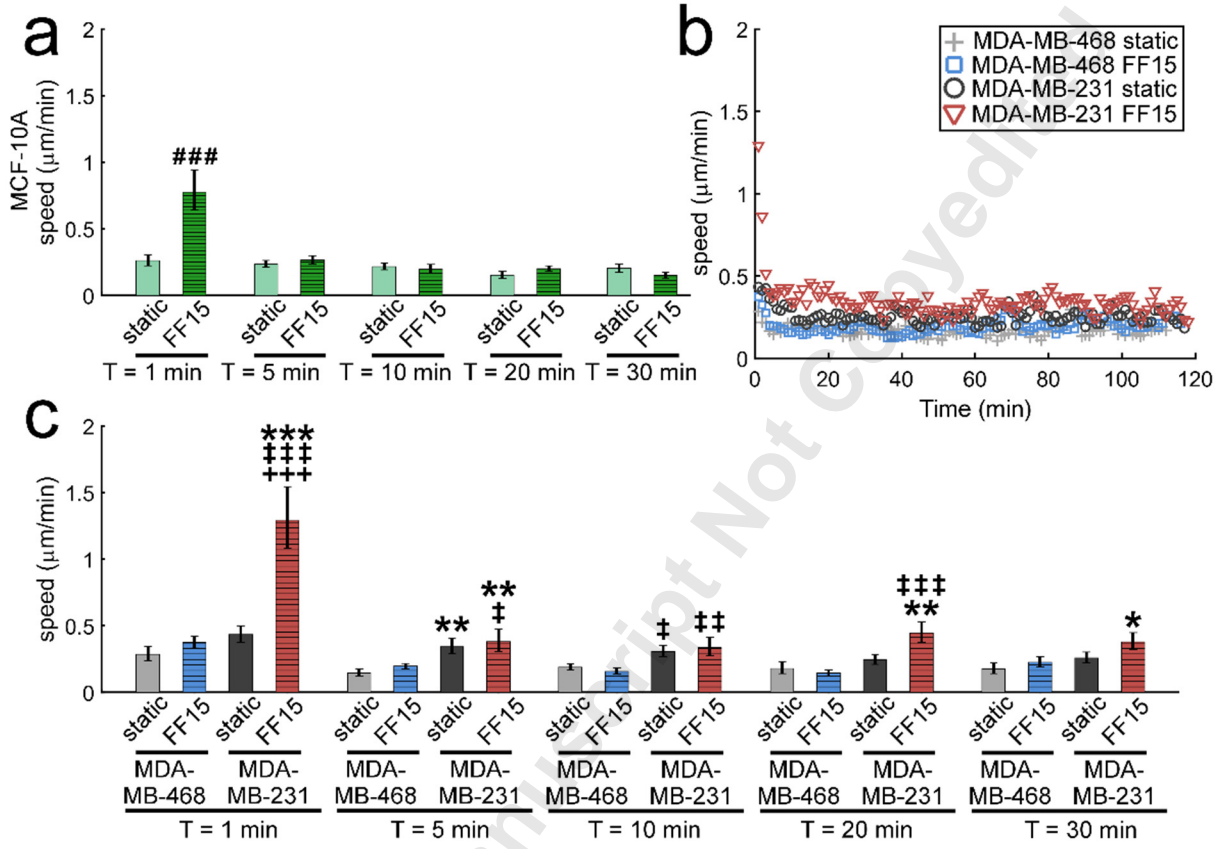

Fig. 4

Journal of Biomechanical Engineering. Received March 08, 2018;
Accepted manuscript posted April 29, 2020. doi:10.1115/1.4047076

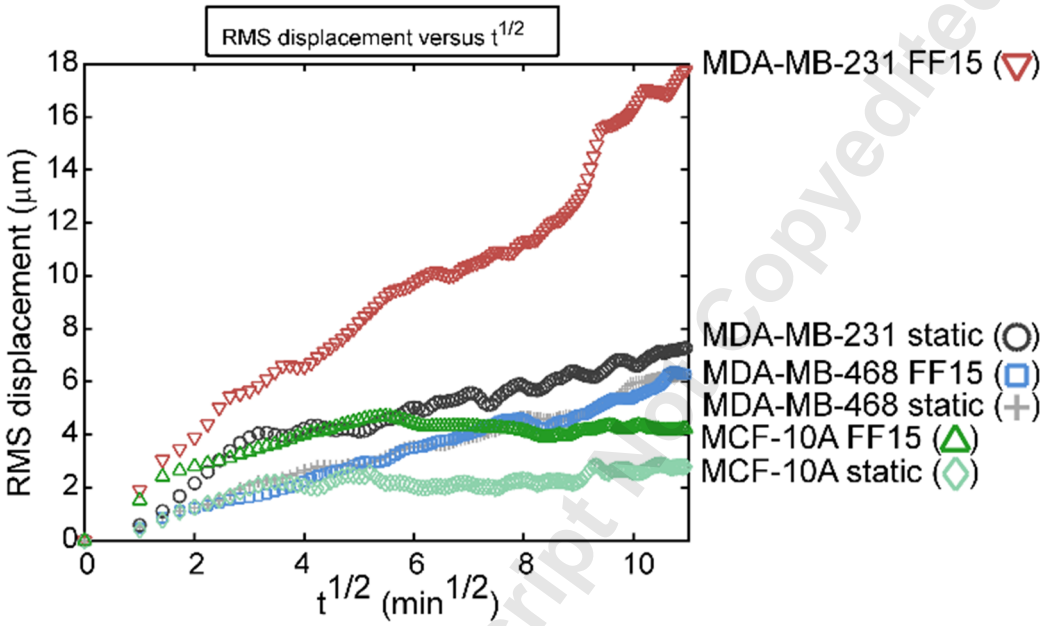

Fig. 5

Journal of Biomechanical Engineering. Received March 08, 2018;
Accepted manuscript posted April 29, 2020. doi:10.1115/1.4047076

The Role of Fluid Shear and Metastatic Potential in Breast Cancer Cell Migration

Brandon D. Riehl, Eunju Kim, Jeong Soon Lee, Bin Duan, Ruiguo Yang, Henry J. Donahue, Jung Yul Lim

SUPPLEMENTARY INFORMATION

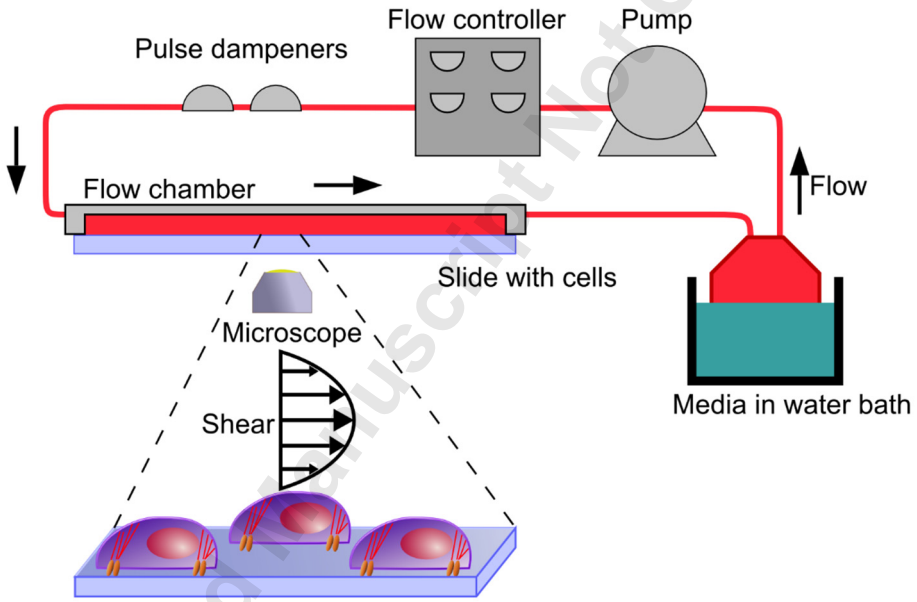

Fig. S1. Schematic of the fluid flow device. Figure is reprinted from our previous publication [14] with permission from the Royal Society.

Journal of Biomechanical Engineering. Received March 08, 2018;
Accepted manuscript posted April 29, 2020. doi:10.1115/1.4047076

Image processing

Table S1. Image processing stack in Time Lapse Analyzer (TLA).

Image processing stack
Sobelfilter Edges (0.04,both)
Dilation (15)
Fill in holes (1000)
Erosion (12)
Opening (12)
Delete small regions (600)

Statistics

Data transforms (Table S2) were applied to correct for data that were not normally distributed to meet ANOVA assumptions.

Table S2. Data transforms applied to cell migration parameters.

Measurement	**Transformation**
Percent of cells migrating with/against flow direction	None
Percent of time migrating with/against flow direction	None
Speed	Log_{10}
Displacement	Log_{10}
Confinement ratio	None
Arrest coefficient	None
Area	Log_{10}

Journal of Biomechanical Engineering. Received March 08, 2018;
Accepted manuscript posted April 29, 2020. doi:10.1115/1.4047076

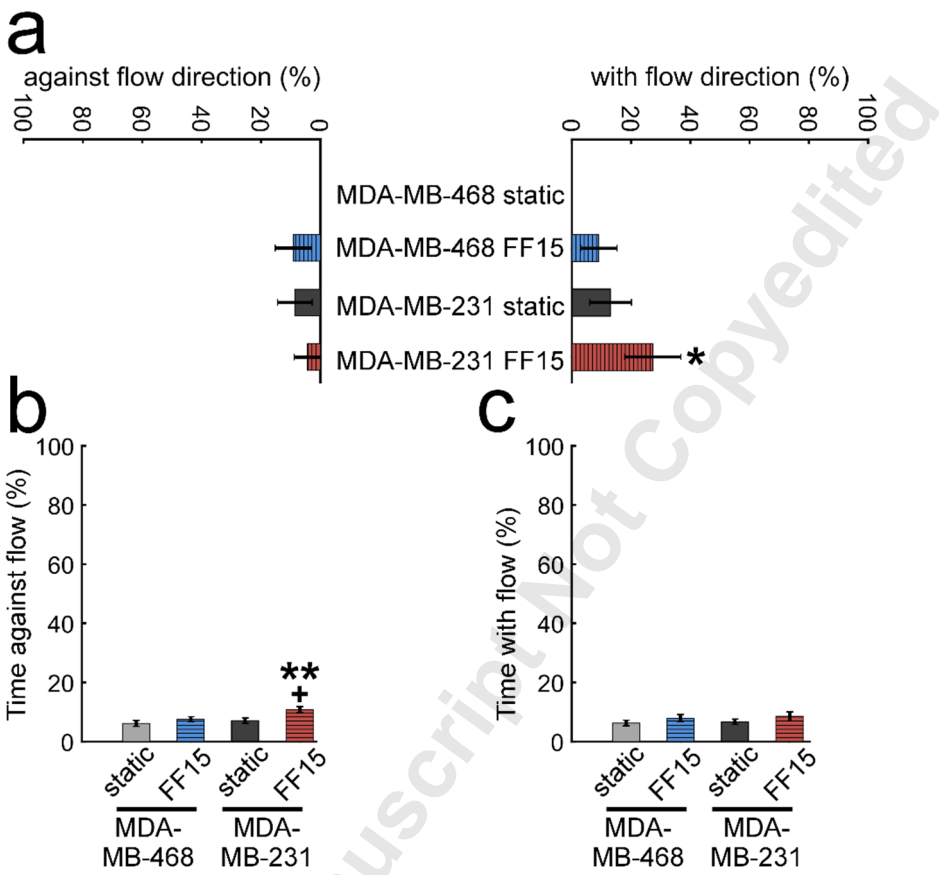

Fig. S2. Trends in migration direction up to 60 min. Halfway through the experiment (t = 60 min), the sheared MDA-MB-231 cell line had the greatest recruitment in the flow direction (a) but also spent the most time migrating against the flow (b). (c) All cells spent similar amounts of time migrating with the flow. *: comparison with MDA-MB-468 static. +: comparison with MDA-MB-231 static. Single and double symbols represent $p < 0.05$ and $p < 0.01$, respectively.

Journal of Biomechanical Engineering. Received March 08, 2018;
Accepted manuscript posted April 29, 2020. doi:10.1115/1.4047076

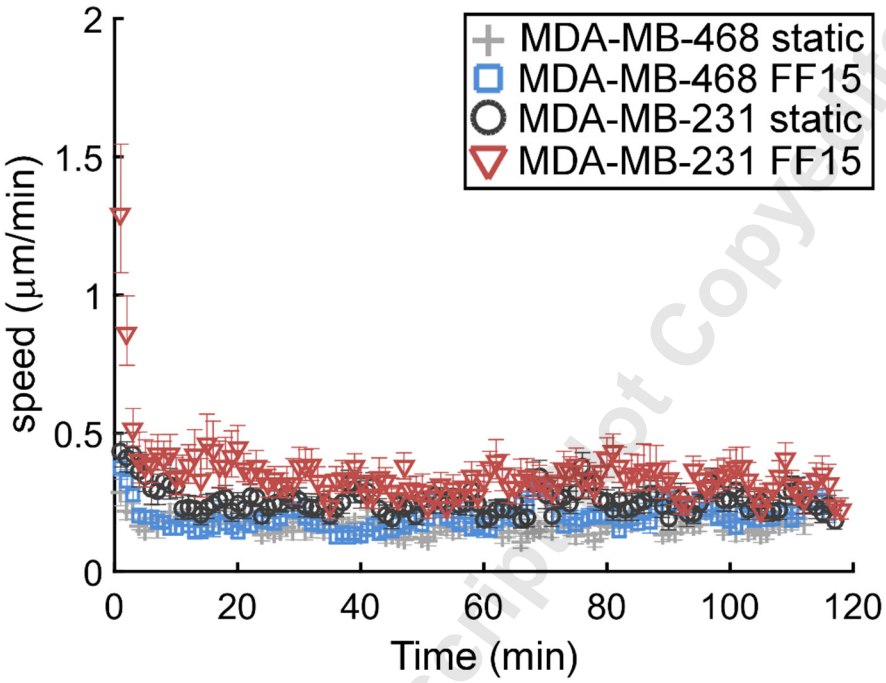

Fig. S3. Average cell speed with error bars. The speed vs. time plot from Fig. 4b is shown here with error bars.

Journal of Biomechanical Engineering. Received March 08, 2018;
Accepted manuscript posted April 29, 2020. doi:10.1115/1.4047076

The mean square displacement (MSD) serves a similar purpose as does the RMS displacement in that it is a measure of the group migration behavior. The difference in MSD is that both time averaging and ensemble averaging are considered [14]:

$$MSD(\Delta t) = \frac{1}{N}\frac{1}{N_{\Delta t}}\sum_{i=1}^{N}\sum_{t_0=1}^{N_{\Delta t}}[x_i(\Delta t + t_0) - x_i(t_0)]^2$$

where Δt is the time step or delay time, N is the number of cells averaged together, $N_{\Delta t}$ is the number of time steps averaged together, and x_i is the cell position vector for the i-th cell. The difference $x_i(\Delta t + t_0) - x_i(t_0)$ is the displacement with time step of Δt starting at t_0. For each time step, cellular displacements are averaged together for each possible starting time, t_0. For example, for a time step of 1 min, the displacement $x_i(2) - x_i(1)$ is averaged together with $x_i(3) - x_i(2)$, and $x_i(4) - x_i(3)$ continuing until all possible starting times, t_0, have been used. This mean is then averaged across all cells in the group to obtain the final MSD. The MSD is then plotted against the time step, Δt (Fig. S4).

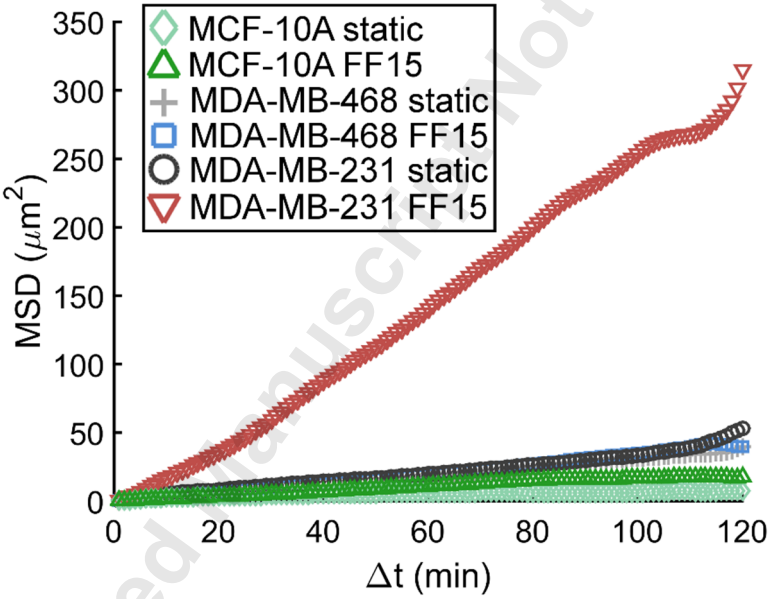

Fig. S4. Mean squared displacement (MSD) plot. The MSD is an ensemble- and time-averaged quantification of group migration. The vastly higher shear-induced migration capabilities of the MDA-MB-231 cells are clearly displayed in this plot.

Journal of Biomechanical Engineering. Received March 08, 2018;
Accepted manuscript posted April 29, 2020. doi:10.1115/1.4047076

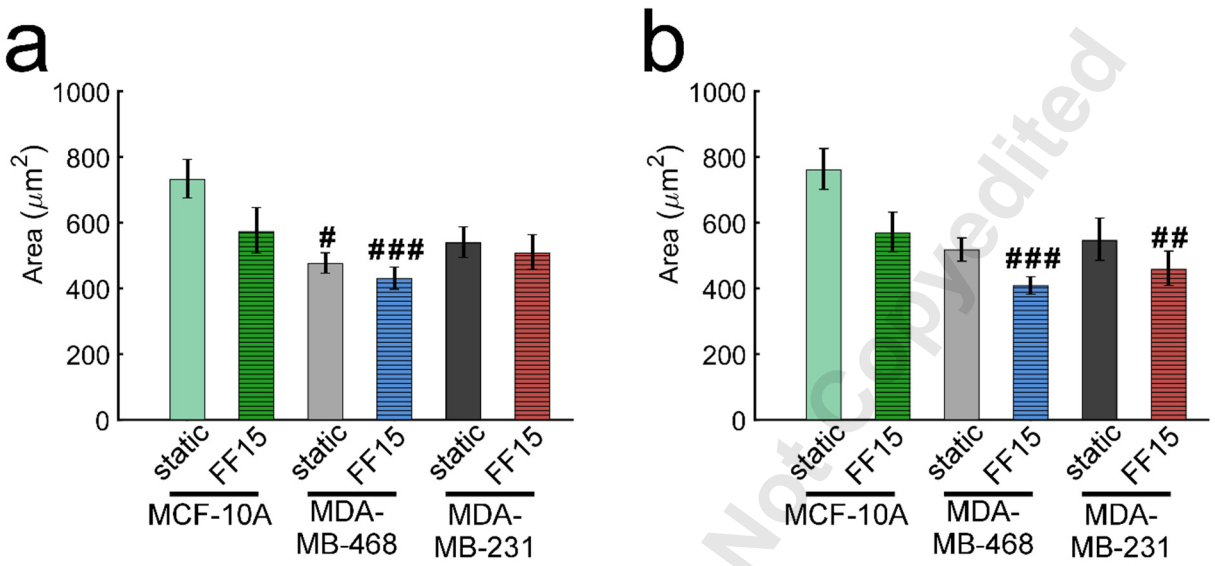

Fig. S5. Average cell spreading area. Cell area at flow onset (a) and at the end of flow (b) did not have significant differences for two breast cancer cell lines. The benign MCF-10A static condition had the largest cell area which remained unchanged during the experiment. **#:** significance with MCF-10A static case with single, double, and triple symbols corresponding to $p < 0.05$, 0.01, and 0.001, respectively.